

# Making Images from Images: Interleaving Denoising and Transformation

Shumeet Baluja<sup>1</sup>, David Marwood<sup>1</sup>, and Ashwin Baluja<sup>2</sup>

<sup>1</sup> Google DeepMind

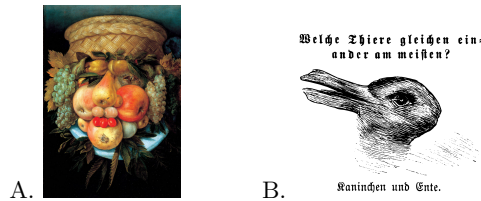
<sup>2</sup> Northwestern University

**Abstract.** Simply by rearranging the regions of an image, we can create a new image of any subject matter. The definition of regions is user definable, ranging from regularly and irregularly-shaped blocks, concentric rings, or even individual pixels. Our method extends and improves recent work in the generation of optical illusions by simultaneously learning not only the content of the images, but also the parameterized transformations required to transform the desired images into each other. By learning the image transforms, we allow any source image to be pre-specified; any existing image (*e.g.* the *Mona Lisa*) can be transformed to a novel subject. We formulate this process as a constrained optimization problem and address it through interleaving the steps of image diffusion with an energy minimization step. Unlike previous methods, increasing the number of regions actually makes the problem easier and improves results. We demonstrate our approach in both pixel and latent spaces. Creative extensions, such as using infinite copies of the source image and employing multiple source images, are also given.

## 1 Introduction and Background

The generation of images that change their appearance under specific transforms, such as rotations, tile rearrangement, and flips, has captivated the minds of visual artists for centuries — exemplified by Salvador Dalí and M. C. Escher. Often grouped broadly as optical illusions, two prominent early examples include the work of Giuseppe Arcimboldo (1590), shown in Figure 1A, and the classic example of the rabbit and duck illusion, shown in Figure 1B. Beyond their artistic appeal as intriguing visual puzzles, these and other optical illusions have been studied for understanding human perception, including intrinsic biases and fundamental cognitive processes [7, 22, 39]. [19, 26] found that modern large-scale image/text embedding systems are also susceptible to illusions (a type of adversarial example [9, 14, 15]).

Within the computer vision community, the quest to create complex visual illusions that can trick the human visual system has encompassed many approaches. For example, *hybrid images* combine the high frequencies from one image with the low frequencies from another to create a hybrid image that appears as one object when viewed close-up and another when viewed from afar [28]. Other work includes creating solids that can be interpreted as different objects



**Fig. 1:** Classic examples of optical illusions. (A) G. Arcimboldo’s *Fruit Basket* (1590) that shows a face when upright, and a fruit basket when upside-down. (B) Depending on the orientation, this image appears either as a duck or a rabbit.

depending on the viewing angle [18, 24] and generating the illusion of motion without movement [11].

Recently, a wide variety of novel work has been conducted in algorithmically creating *photo-realistic* optical illusions. The foundation of almost all of this work is the text-to-image generative models [6, 8, 23, 27, 30, 32–34, 36] that have become the de facto standard method to synthesize high-quality images from text prompts. To gain more fine-grained control of the generation process, as is necessary for creating illusions, a variety of methods have been proposed that either replace or modify specific objects in the generated images or manipulate the style of generation [2, 10, 27, 38]. Samples of our work, shown in Figure 2, provides a novel mechanism for controlling the generation of images.

In work close to ours, Tancik used diffusion to simultaneously denoise multiple views of the same image [37]; two different user-specified subject were visible by rotating the image. Geng *et al.* [12] significantly broadened those results by showing that any pre-specified rearrangement of pixels is a suitable transformation that can be captured by the simultaneous denoising processes. They used multiple prompts within a pixel-based diffusion system, DeepFloyd [35], to create a single image that, through pre-specified transforms, represented the multiple prompts. An alternative approach [4] used Stable Diffusion [32] to create similar rotation illusions as well novel overlay illusions in which multiple realistic images are overlaid to reveal an image of a new subject matter. In 2024, a broadened set of transforms was presented by [13]. This included automatically generated photo-realistic hybrid images (of the type that were first presented in 2006 [28]), in which a single image appears as different objects at different scales.

A limitation of all of the previous work is that it has been confined to a narrow problem scope: multiple images were generated simultaneously to ensure closely compatible content under the pre-specified transforms [4, 5, 12, 13, 21]. Let us consider a more difficult problem. Imagine that we are given a source image, such as the artwork in Figure 2 (top row), and our goal is to create images that depict entirely different subjects using only tiles from the source. Using a static source image under the constraints of a pre-specified transform (as in previous work) does not work. The result is already fully determined and is not dependent on the prompt.



**Fig. 2:** Through simple tile permutations, a source image can be converted to a new image of any subject matter. Both the permutation and the content are learned simultaneously; the images created are suited to the tiles available for the composition. Examples with three famous paintings are shown. Each is converted into 3 different subjects (two results are shown for each). The number of tiles that the source is divided into is  $64 \times 64$ ,  $32 \times 32$  and  $16 \times 16$  (top to bottom). With our approach, as the number of tiles grows, the *easier* it is our for system to produce compelling results; the opposite is true for state-of-the-art alternate systems.

To tackle this problem, we must first create a method to allow the transformation to be dynamically discovered. Second, even with dynamic transforms, we note that the constraints on the images to be created are much tighter with a static source image than one that can be co-created. In this new formulation, we can only create the new image with the tiles from the first; arbitrary pixel colors are not possible. Put another way, there is more freedom in finding compatible pixels for both images when the pixel values are not pre-determined.

The closest previous work that bridges the studies with optical illusion creation and our tightly constrained diffusion process is by Bar-Tal *et al.* [3]. There, the constraints on multiple simultaneous diffusion processes are maintained to seamlessly extend and blend multiple images. This was used for creating panoramic images and region-based content modification. Additionally, we note that [13] also used real images as one target stage for their hybrid-image illusions. They exploited the visibility differences of high and low frequency features at different resolutions - a very different approach and goal than ours.

As will be described next, our method does not require a pre-specified arrangement of tiles, but instead determines the optimal permutations dynamically

as the new image content is generated. This dynamic patch matching technique employs the *Hungarian Method* [20], also known as the *Kuhn-Munkres* [25] algorithm, for optimal assignment. The image transformation process is modeled as an optimization problem with shifting constraints and is addressed by alternating steps of image diffusion and energy minimization. We also extend our method to cases employing infinite copies of the source image, providing a powerful tool for generating diverse and visually appealing images from a single starting image.

Finally, we will show how the general approach of interleaving diffusion and energy minimization steps can be extended to other image transformations beyond tile rearrangement.

## 2 Diffusion and Constrained Optimization

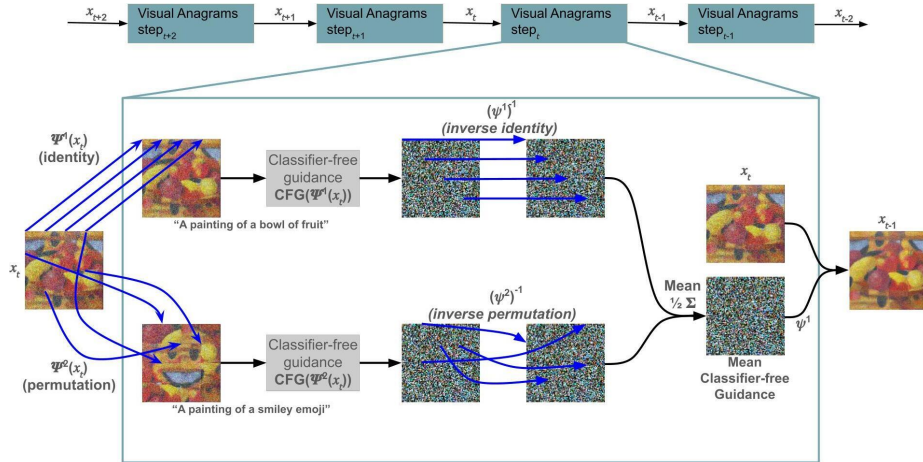
To address the task of using a static source image for creating a new image, we first reformulate the more general task of simultaneously denoising two non-static images. We employ a diffusion process [16] common to text-to-image systems that denoises an image over  $T$  steps, starting from pure noise:  $x_T \sim \mathcal{N}(0, 1)$ .  $t$  proceeds from  $T$  down to 0.  $x_t$  is the input to step  $t$  which produces  $x_{t-1}$ , an image with less noise, as the input to the next step.  $x_0$  is the final output of diffusion: the fully denoised image. By incorporating deep neural networks with classifier free guidance [17] to predict the noise at each step, the diffusion process gradually changes pure noise into an image described by a text prompt,  $p$ .

We base our system on Visual Anagrams [12] which uses diffusion to synthesize  $N$  images from  $N$  different prompts such that the images at step  $t$  are the same under the inverse of each transformation  $\psi^i$ , denoted  $\psi^{i^{-1}}$ . The corresponding pixels in the images, as determined using  $\psi^i$ , are exactly the same. For simplicity, going forward, we will define the first of  $N$  diffusion inputs to be the input image,  $x_t$ . The remaining diffusion inputs can be derived from the first as  $\Psi^i(x_t) = \psi^i(\psi^{1^{-1}}(x_t))$  where  $1 \leq i \leq N$  ( $\Psi^1$  is identity)<sup>3</sup>; see Figure 3. In [12], they *a priori* select the transforms,  $\psi$ . To synchronize the  $N$  parallel diffusion processes, the computed guidance for each prompt is averaged at each step.

For the majority of this study, we will concentrate on transforms,  $\psi$ , that divide the image into  $M \times M$  tiles and permute the tiles intact rather than treating pixels individually.

As a baseline, we show results obtained by using the approach in [12] using  $N = 2$ , see Figure 4. As in [12],  $\psi^1$  is an identity function and  $\psi^2$  is a randomly chosen tile permutation. Also, to match their studies, we use the pre-trained diffusion model DeepFloyd [35] that operates directly on pixels. Our qualitative observations of the results match those in [12]: prompts that allow more room for interpretation, such as “a painting of.” perform better than those with strict expectations, *e.g.* “a photograph of.” Additionally, the broader the query, the higher the likelihood of a pleasing result, *e.g.* the pair (“a car” and “a tree”) will appear better than the pair (“a red Mustang” and “a willow tree”).

<sup>3</sup> This definition of  $\Psi$  provides generality. If one is willing to restrict  $\psi^1$  to identity then  $\Psi^1(x_t) = \psi^1(x_t)$ .



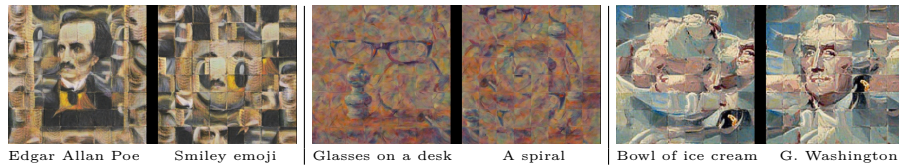
**Fig. 3:** A description of a Visual Anagrams step, adapted from [12], using  $N = 2$ . A single image that appears as a bowl of fruit can be subdivided into  $4 \times 4$  square tiles and rearranged into a “smiley face” emoji. To create this, two transforms of the same image (here  $\psi^1$ =identity and  $\psi^2$  is a permutation of  $4 \times 4$  tiles) are denoised simultaneously. Two diffusion processes use different prompts to create their per-pixel classifier-free guidance (CFG), represented here as an image. The CFGs are passed through their respective inverse transforms into a shared space and averaged before being applied to input  $x_t$ . Both images contribute to the guidance and remain synchronized.

The most immediate limitation of [12] is that the transformation function (the permutation) is static and selected prior to starting the process. To elucidate the concern, consider the pair of prompts (“beach sunset”, “basketball”). It is easy to imagine that the color and shape of a basketball can be used for orange skies and a setting sun. However, if the randomly chosen tile assignment is incompatible with such a layout, either a less likely image is generated or the objects in the image may appear incorrect. Next, we address this problem.

## 2.1 Simultaneously Learning Permutations and Images

It is impossible to know *a priori* what the suitable permutations for a set of prompts will be. We will develop a procedure that allows the transformation permutation to change such that the permutations are selected that best match the images. Before proceeding, it is important to state the intrinsic “chicken-and-egg” problem. If the two final images were known, we could calculate the best permutation in advance. However, the two images are being synthesized simultaneously along with their permutations. Therefore, we need to repeatedly re-optimize the permutation as the image is synthesized.

We find the permutation using *dynamic matching*. Consider two images, each composed as a grid of  $M \times M$  non-overlapping tiles of equal size. The distance between tiles is their  $L_2$  pixel distance, though more elaborate mechanisms such as perceptual similarity metrics can also be employed [1]. The goal is to assign



**Fig. 4:** In each pair, each image is  $192 \times 192$  pixels. Each image can be subdivided into a grid of  $8 \times 8$  (64 total blocks) of  $24 \times 24$  pixels. For each pair of images, there is a permutation of the 64 blocks that transforms the left to right and vice-versa. As in [12], the permutation is pre-specified and chosen randomly. To show [12] in the best light, these are the top performing, as judged by their CLIP scores (distance to prompt) [29]. All prompts were preceded by “A painting of”.

each tile in the first image to exactly one distinct tile in the second such that the total summed distances of assignments is minimized. This can be characterized as a complete bipartite graph  $(S, T; E)$  where vertex sets  $S$  and  $T$  represent tiles in the first and second images and  $E$  has an edge distance equal to the distance between its endpoint tiles. The solution is a perfect matching (a matching where each vertex has exactly one edge) that minimizes the total edge distance. This formulation will be used again in Section 5.1.

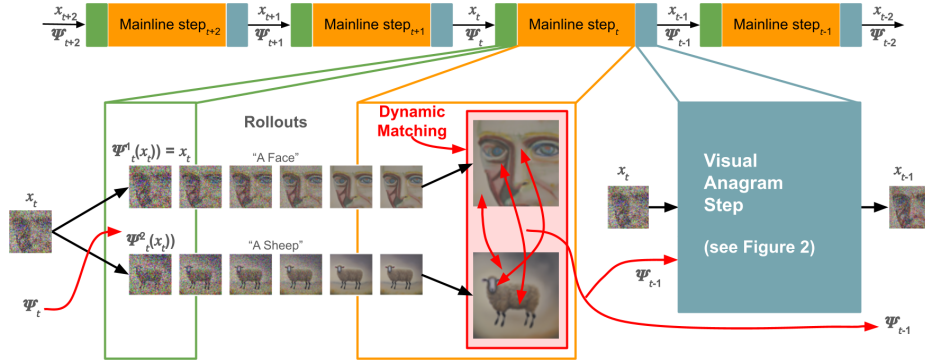
To compute this, the tiles of each image are flattened to an array of length  $M^2$  and the distances between every tile in the first image and every tile in the other image are arranged in a matrix,  $D$ . We permute the rows of  $D$  to minimize its trace.

$$\min_P \text{tr}(PD) \quad (1)$$

where  $P$  is a permutation matrix, a  $(0,1)$ -matrix with exactly one 1 in each row and at most one 1 in each column, with the same shape as  $D$ . This assignment problem is optimally solved in polynomial time using the Kuhn-Munkres algorithm [20, 25].  $\psi(Q)$  implements the tile assignment  $P$  on the pixels of  $Q$ .

We incorporate dynamic matching as part of the “mainline”, the sequence of “Visual Anagrams steps” described so far. Its role is to update the matching tiles between Visual Anagrams steps as the images are created. Specifically, dynamic matching updates  $\psi$  at step  $t$ , referred to as  $\psi_t$  (and similarly  $\Psi_t$ ), to  $\psi_{t-1}$ . A naive approach is to simply recalculate the assignment in  $\psi$  at each Visual Anagrams step; however, this was unstable – likely because matching noisy images in the beginning (closer to  $t = T$ ) resulted in unhelpful assignment changes.

To address this, we introduce a “rollout” at the beginning of each mainline step. A rollout is an *entirely separate* diffusion process starting from  $\Psi_t^i(x_t)$  and stepping forward  $l$  steps as a form of lookahead approximation to the *a posteriori* image for each prompt. (Numerous values were tested for  $l$  and, experimentally, we found a lookahead of 5 steps was sufficient.) This approximation outputs an “idealized” image to show where each prompt *would* lead if used in diffusion *independently*. We then use dynamic matching *on the idealized images* to compute

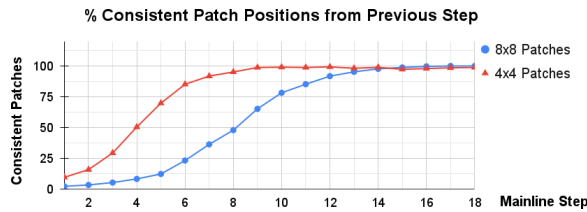


**Fig. 5:** Incorporating dynamic matching between each diffusion step. In the green rectangle, the input image is permuted and the rollout occurs. In the orange rectangle, the images created at the end of the rollout are used to compute the new permutations through dynamic matching.

new tile assignments; this produces the new  $\psi_{t-1}^i$  and  $\Psi_{t-1}^i(x_{t-1})$ . As shown in Figure 5, the  $N$  rollouts take  $\Psi_t^i(x_t)$  as input and the mainline step outputs  $x_{t-1}$ .

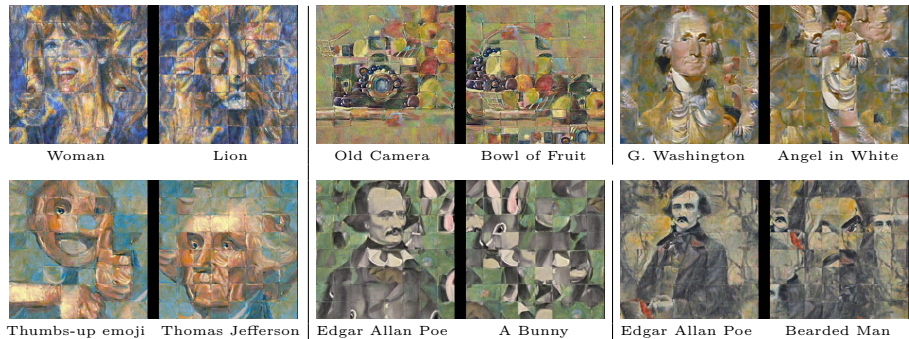
After the dynamic matching step, the idealized images are discarded; only the new assignments are maintained. The Visual Anagram step proceeds as usual, using  $\Psi_{t-1}(x_t)$  as input<sup>4</sup> and outputs  $x_{t-1}$ ; see Figure 5.

It is interesting to examine, on a running system, how the dynamics of the tile permutations change across mainline steps. Figure 6 shows that the number of changes in tile assignments rapidly reduces. This occurs because, as the mainline steps proceed, the output images of each of the rollouts get closer to the final output (and thereby change less between iterations); therefore, the optimal matches between the rolled-out images cease shifting.



**Fig. 6:** As the diffusion process continues, changes between successive permutations is reduced. As the images become more consistent (as  $t \rightarrow 0$ ) each  $\psi_{t-1}$  looks more like  $\psi_t$ . By iteration 15, the  $8 \times 8$  tiles have ceased movement. Movement ends by iteration 9 for the  $4 \times 4$  tiles. Average of 10 runs shown.

<sup>4</sup> More precisely, the diffusion process inputs are  $\psi_{t-1}^i(\psi_t^{1-i}(x_t))$ . However, any set of transforms  $\psi$  can be equivalently restated without changing  $\psi^1$ ; thus,  $\psi_t^1 = \psi_{t-1}^1$ . By substitution, the diffusion process inputs are  $\psi_{t-1}^i(\psi_{t-1}^{1-i}(x_t))$  which is just  $\Psi_{t-1}^i(x_t)$ .



**Fig. 7:** The transformation is dynamically determined as the image is created. Note that the same prompt (Edgar Allan Poe), when paired with different prompts, yields different images because of the constraints imposed by the pairing.

Qualitative results with dynamic matching are shown in Figure 7. To provide a quantitative measure of quality, 1200 trials were conducted, half with dynamic matching and half without. Each trial synthesized an image based on two prompts (randomly chosen nouns). The distance of the resulting images to their respective prompts was measured in the CLIP embedding space [29]. For  $4 \times 4$  permutations, dynamic matching averaged 22.39 distance and 22.43 without. The statistical difference, measured with the non-parametric Wilcoxon paired significance test, is ( $p < 0.05$ ). For  $8 \times 8$  permutations, the results were 22.36 and 22.40, with significance ( $p < 0.01$ ).

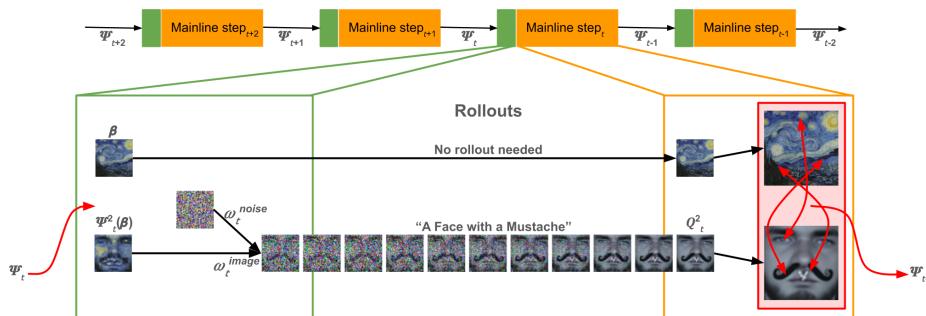
In summary, by employing this novel matching between Visual Anagrams steps, we discover the tiles that are similar in appearance in the synthesized idealized images, and tie them together. We no longer need to adhere to randomly chosen ties. Revisiting the “basketball” and “beach sunset” example and using dynamic matching, tiles that are orange in the separate images may be tied together, regardless of where the original random permutation placed them. Next we show how this capability allows us to tackle a new range of tasks.

### 3 Using a Known Source Image

In the previous section, dynamic matching allowed us to generate multiple images from multiple prompts while progressively discovering the optimal tile assignments between them. Here, we exploit this new freedom to *a priori* specify the tiles that all the images must contain. The tiles can be taken from any “source” image; if the *Mona Lisa* is used, then the generated images will only use its exact tiles.

Starting with a source image changes the task from finding the RGB-pixel values to rearranging the tiles of the source image to create a new image described by the specified prompt. On first glance, this may seem like a trivial problem: given the *Mona Lisa*, find the tiles that best match another image, such as an image of a dog. However, this *is not* what is being done here. Instead, we are





**Fig. 8:** With a fixed image,  $\beta$ , the rollout procedure with an additional noising step is used to replace both the mainline and rollout procedures described in the previous section. In this example, an image of a man with a mustache is created by moving tiles around from Van Gogh’s *Starry Night*. Also, note that we no longer need to keep  $x_t$ ; instead,  $x_t$  is directly computable from  $\Psi_t(\beta)$ .

creating an image of the dog that is well suited to the images allowed by the (e.g.  $16^{2!}$  for the  $16 \times 16$  tile case) permutations of the *Mona Lisa*’s tiles.

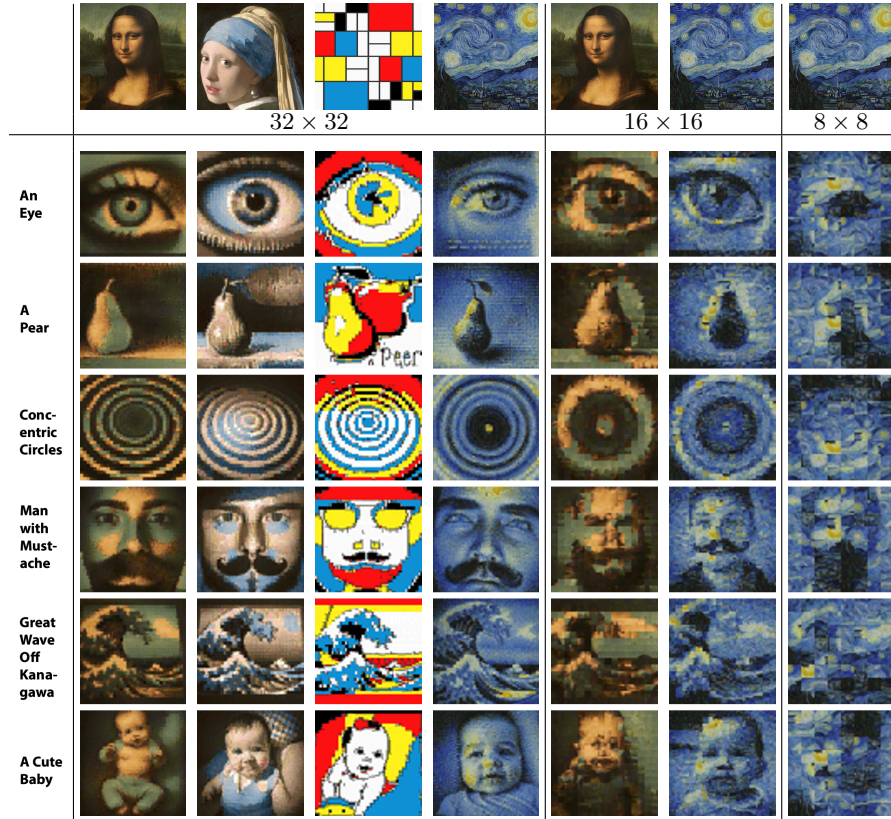
To use a source image,  $\beta$ , as the basis for the image creation, we start with the method described in the previous section. Since we no longer need to determine the actual values of the pixels (only where the pixels will be moved from the source), we can simplify the process. Within the context of the procedures shown thus far, we set the first image to  $\beta$  and the prompts start at  $i = 2$ ; see Figure 8. The salient differences between the previous procedures and the current are:

1.  $\psi_t^1$  is set to the identity function.  $x_t$  is no longer an input since all rollout inputs can be derived as  $\Psi_t(\beta)$ .
2. Given  $\psi_t$ , we directly compute  $\Psi_t(\beta)$  for initialization. Recall that  $\Psi_t^i(\beta)$  is a permutation of a noise-free source image. For a rollout to be useful (since rollouts use diffusion internally), it expects a noisy image, not one that is noise-free. Therefore, we *re-add* noise to  $\Psi_t^i(\beta)$  to create the rollout input, a process termed “rollout mixing”. We can characterize rollout mixing as:

$$w_t^{image} \Psi_t^i(\beta) + w_t^{noise} \epsilon \quad (2)$$

where  $\epsilon \sim \mathcal{N}(0, 1)$  is noise.  $w_t^{image}$  and  $w_t^{noise}$  for step  $t$  are computed directly from the diffusion schedule (see [16, 32] for details). An effect of the diffusion schedule is that, the earlier in the mainline process, the more weight is given to  $w_t^{noise}$ , allowing larger changes.

3. We perform each rollout (see Figure 8) to completion, which yields an idealized noise-free image that we call  $Q_t^i$ . The tiles in  $Q_t^i$  are matched with  $\beta$  revealing the new  $\psi_{t-1}$ . This is analogous to the matching process earlier, where we matched to the first idealized image.
4. Once dynamic matching has computed the new assignment of tiles, there is no further need to adjust the pixel values. They are directly taken from  $\beta$ . The Visual Anagram step is no longer required.



**Fig. 9:** Examples using fixed source images. Top Row is the original image ( $\beta$ ), the bottom 6 rows shows the images created by permuting the tiles in  $\beta$ . Examples are shown for  $32 \times 32$  to  $8 \times 8$  tiles; the exact same pixels as the original are used.

Results with square crops of four paintings (da Vinci’s *Mona Lisa*, Vermeer’s *Girl with a Pearl Earring*, a Mondrian-like artwork, and Van Gogh’s *Starry Night*) used as the source image,  $\beta$ , are shown in Figure 9. Each artwork is converted to 6 new subjects. When  $\beta$  contains a variety of natural shading artifacts, performance is vastly improved. Conversely, when  $\beta$  has few colors and no shading (column 3), the results are more akin to clip-art. As we increase the number of tiles, quality improves. The use of a predetermined source image significantly amplifies the constraints, thereby exacerbating the complexity of the problem; fewer tiles than  $16 \times 16$  produced inferior images. One of the subtle, but most interesting, findings in these results is that since the same seed was used to generate these images, the differences in the images of each row is due to the constraints imposed by matching the source image. A visualization of how rollouts progress is shown in the Appendix.

To this point, we have demonstrated our approach with two prompts. However, that is not a limitation of the procedure. In fact, with the use of a  $\beta$  image, it can be shown that  $N$  prompts need not be solved simultaneously. Instead, equivalent results will be achieved when, using  $\beta$ , each of the  $N$  prompts is solved independently. This will yield images that are transforms of each other.

## 4 Working in Latent Spaces

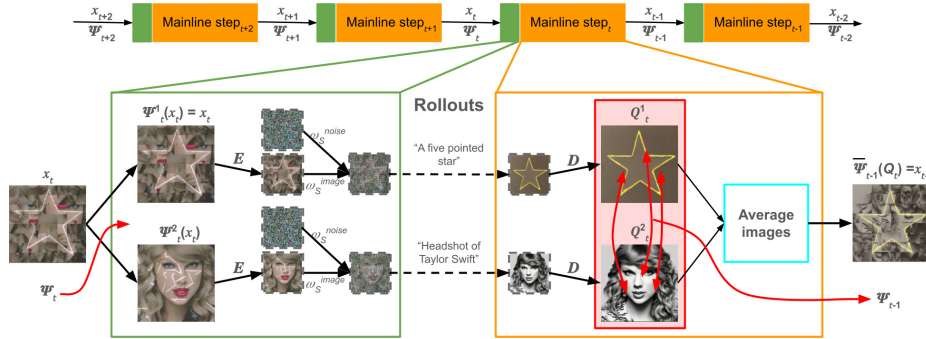
To this point, we have used DeepFloyd to allow direct comparison to [12], but its pixel-based representation of  $x$  is uncommon in modern diffusion systems. Since latent diffusion-based systems are rapidly progressing in quality, we have also extended our system to work with latent diffusion systems, specifically Stable Diffusion’s version 2.1 (SD 2.1) [31]. Rather than operating directly on pixels, the diffusion of  $x_t$  is in a more compact “latent” representation that can be encoded and decoded from/to pixels by using a pre-trained encoder and decoder, both of which are a core part of all pre-trained latent-diffusion systems.

Upon first glance, the simplest approach in using a latent diffusion system would be to simply translate all the mechanisms with DeepFloyd directly, and work entirely in latent space, with a decode only for the final output. However, latent diffusion introduces two significant challenges. First, as witnessed in [12], transforms on the latent representation may not preserve spatial characteristics. This problem is exacerbated by dynamic matching, which also occurs in the pixel-space. Second, latent diffusion is hyper-sensitive to early stages of denoising; rolling out from intermediate steps produces little change in the idealized image.

We closely follow the steps in Section 3 and introduce modifications as necessary. As before, the rollout mixing step adds noise before the start of each rollout. Each rollout proceeds 50 steps,  $S = 50$ . (While 50 steps is more than we used with DeepFloyd, we empirically found this to be necessary with latent diffusion.) We keep the mainline steps at  $T = 15$ , sufficient to reach convergence. As before, the output of each rollout is labeled  $Q_t^i$  and it is a noise-free idealized image.

Experimentally, we found that latent diffusion solidifies many characteristics of the final image in the very early diffusion steps. Starting a rollout with higher fractions of the image (as opposed to noise), as we did with DeepFloyd, causes output  $Q_t$  to be too similar to the rollout input. This prevents rollouts from creating novel images and eliminates their usefulness. To allow the rollout enough freedom to create new images, we always start rollouts from the beginning of the diffusion process (*i.e.*  $s = 50 \rightarrow s = 0$ ). To do this, we start with rollout mixing:  $w_S^{image} \Psi_t^i(x_t) + w_S^{noise} \epsilon$  using a “mixing ratio”  $\frac{w_S^{image}}{w_S^{image} + w_S^{noise}}$  of 2%. At 2%, the image provides enough direction when combined with the noise to influence the rollout, but not too much so as to limit the rollout’s ability to change the input. Numerous other values were tried; ranges of 1 – 4% were most often successful.

Once the idealized image has been created, it is again tempting to simply translate all the mechanisms with DeepFloyd directly, and work entirely in latent space, with only a decode for the final output. However, the dynamic matching



**Fig. 10: Changes for latent diffusion.** Latent representations, with a dashed outline, are used for diffusion and pixel images are used for dynamic matching and calculating  $\Psi$ . Latents are decoded with  $D$  for dynamic matching then re-encoded with  $E$ ;  $D$  &  $E$  are pretrained components of the latent diffusion system. Rollout mixing uses fixed  $w_S^{image}$  and  $w_S^{noise}$ . Rollouts span a full diffusion run from  $s = 50$  to  $0$ .

is spatial over pixels – *i.e.* in the decoded image space. To perform the matching, we must, therefore, decode the output of each rollout to produce the pixels for  $Q$ , the input to dynamic matching. See Figure 10.<sup>5</sup>

We note that it is important to consider when to add noise (Figure 10). One choice is to add noise to the pixel image and then encode; however,  $E(\Psi_t^i(w_S^{image} x_t + w_S^{noise} \epsilon))$  doesn’t guarantee the noise component is preserved as  $\mathcal{N}(0, 1)$  in latent space. Instead, we add noise *after* encoding. The input to each rollout is therefore:  $w_S^{image} E(\Psi_t^i(x_t)) + w_S^{noise} \epsilon$ .

An additional implementation detail: when using dynamic matching, the first image  $Q_t^1$  is used to produce  $\psi_{t-1}$  (see red box in Figure 10). We experimented with using  $\Psi_{t-1}^1(Q_t^1)$  as the output of the mainline step. However, we found that using an average of the rollout outputs worked a bit better:

$$\bar{\Psi}_{t-1}(Q_t) = \psi_{t-1}^1 \left( \frac{1}{N} \sum_{i=1}^N \psi_t^{i-1}(Q_t^i) \right) \quad (3)$$

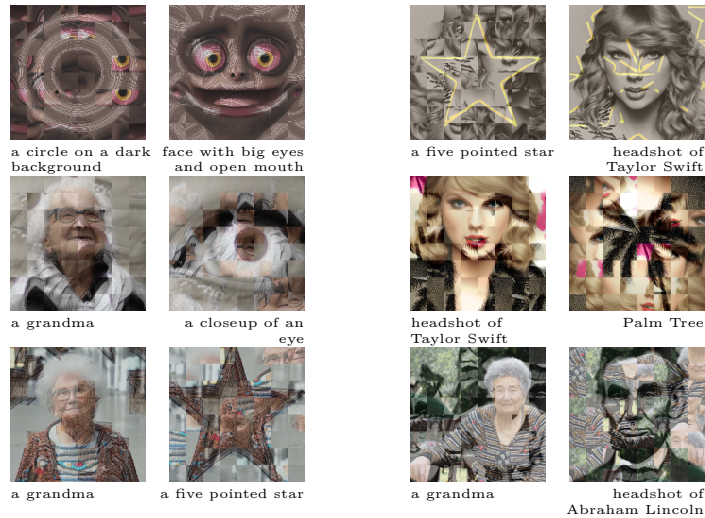
This may be due to the specifics of the diffusion process (SD 2.1) and may be switched back when other systems are employed.

Examples created using latent diffusion are shown in Figure 11. Perhaps the most evident difference between these images and the results with DeepFloyd is in the quality improvement. The latent diffusion model tends to produce clearer images than DeepFloyd, with far less structured noise and more distinct edges. The overall improved quality of the images with respect to the fidelity to the prompt is reflected in the lower CLIP distances: 21.0 for the (4x4) and 21.0 for

<sup>5</sup> Note, despite being “latent” features, their commonly employed spatial layouts lends themselves to encoding spatially localized information. Therefore, we conducted experiments performing the transformations directly in the latent spaces. However, these *did not* produce as compelling results.

the (8x8); both are statistically significantly lower ( $p < 0.01$ ) than the results with DeepFloyd.

Figure 12 gives a demonstration of how our system scales with multiple images and large number of constraints. Unlike previous systems where the larger number of tiles and prompts severely degrade performance, the larger number of tiles provides our approach more degrees of freedom for better results. Figure 13 also shows results with 5 prompts, with prompts chosen to present a clear visualization of how each image affects all the others by propagating constraints (in this case most clearly colors).

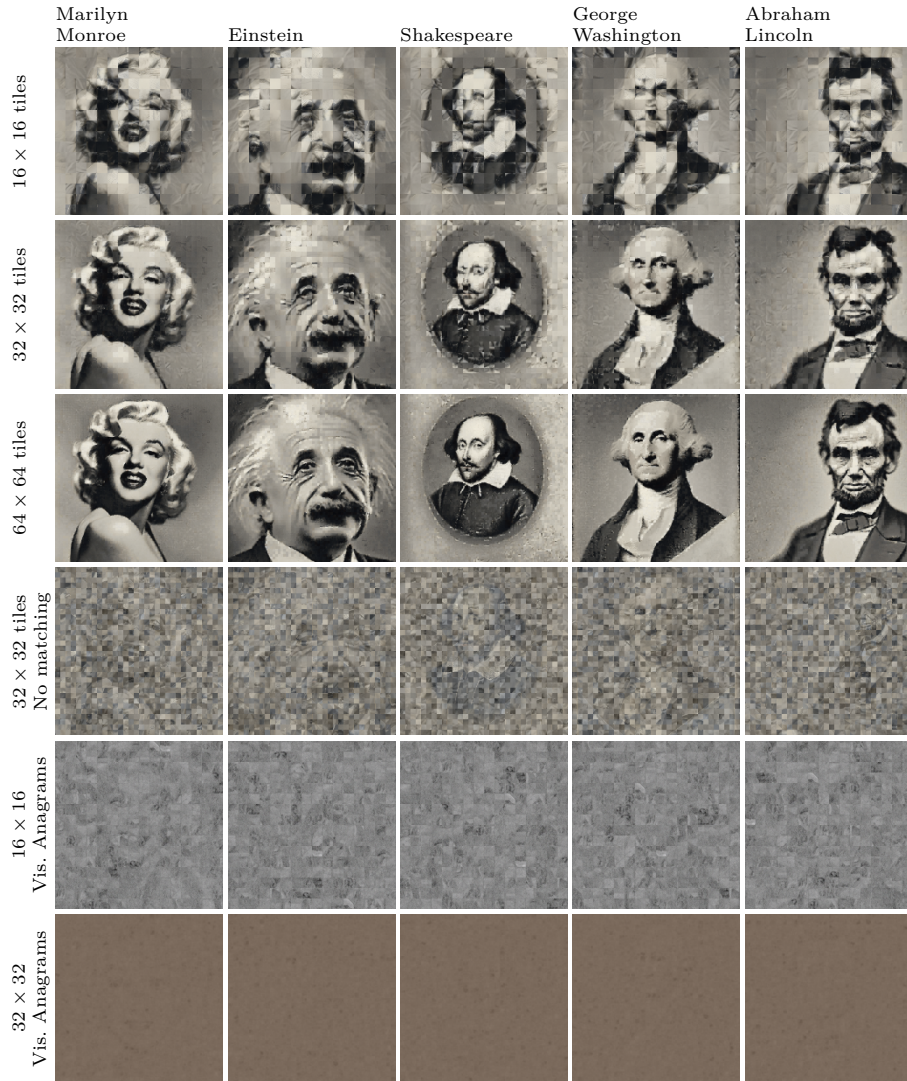


**Fig. 11:** Examples created using latent diffusion. The output images are  $768 \times 768$  pixels. The left of each image pair is divided into an  $8 \times 8$  grid of tiles that are permuted to get the image on the right. We repeat the same prompt with different pairs to show the effects of the constraints imposed by the parallel diffusion processes.

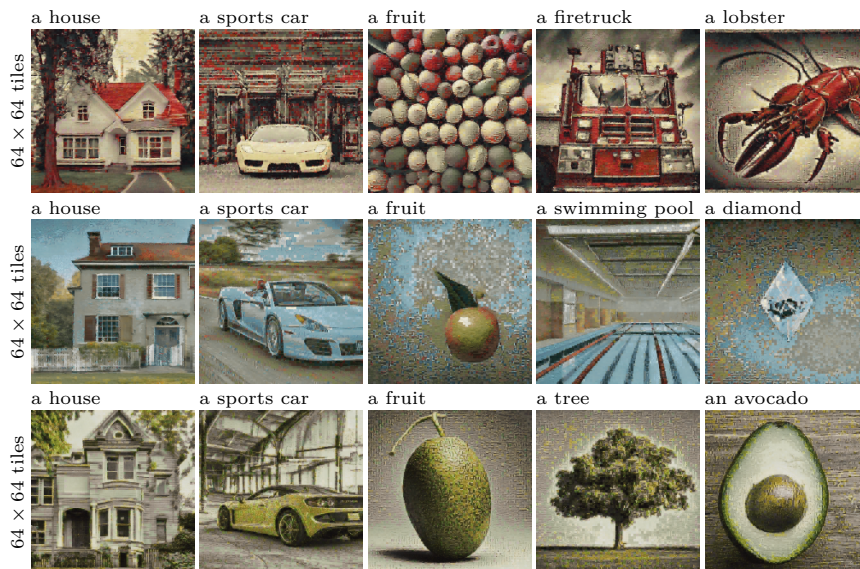
### 4.1 Known Source Image

Analogous to Section 3, we describe how to use an *a priori* specified source image within a latent diffusion-based system. We continue to use the same overall settings as the latent diffusion described above: we retain the full independent rollouts of length  $S = 50$  as well as the 2% rollout mixing ratio.

In order to accommodate the source image, we note that  $Q^1$  is set to  $\beta$ . As earlier, there is no rollout required for the source image. Importantly, unlike Section 3, where we *switched* to explicitly adding noise back into  $\Psi^2$  (Figure 8), we note that the latent diffusion system already uses this approach, so this



**Fig. 12: Multiple prompts comparison.** The images in a row use the same tiles. The images are  $768 \times 768$  pixels and the tiles are  $48 \times 48$ ,  $24 \times 24$  or  $12 \times 12$  pixels in image rows 1, 2 and 3, respectively. “No matching” skips the dynamic matching. “Vis. Anagrams” uses the implementation from [12]. To show each systems at their best, the Visual Anagrams system prepended “a painting”, and ours prepended “a photograph of”. Most interestingly, without dynamic matching, there is only a barely perceptible resemblance to the prompt; instead, the easiest matches are large fields of consistent color, with only minute variations to reflect the prompt. In contrast, with dynamic matching, the images appear bright and easily recognizable.



**Fig. 13:** A visual demonstrations of how constraints are propagated through the parallel diffusion processes. In these three examples that use 5 prompts, 3 prompts are kept constant, while the last two are changed. The last 2 prompts have strong colors associated with them. Notice how the prototypical object’s colors specified by the last 2 prompts is visible in all 5 images – an effect of constraint propagation.

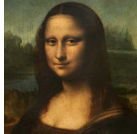

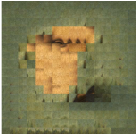







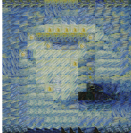



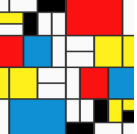

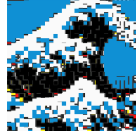

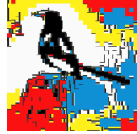



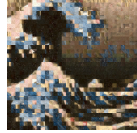
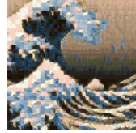




requires no further change. The final outputs are the images  $\Psi_0(x_0)$ . Results are shown in Figure 14 under copies=1.

## 5 Creative Extensions

### 5.1 Infinite Images and Multiple Basis Images

In Section 2.1, we characterized the tile assignment as a perfect matching. However, when using a fixed source image, we can consider an interesting variant – what if we had  $c$  (where  $c$  could be infinite) copies of the source image,  $\beta$ , and could select the tiles to use from any of the copies? In this scenario, as before, every tile in the permuted image must be assigned to a tile in  $\beta$ , but not every tile in  $\beta$  needs to be used. This can be characterized as a matching in a bipartite graph  $(S, T; E)$  where vertices  $S$  contains  $c$  vertices per fixed image tile and  $T$  contains the tiles of the permuted image. The solution is a (non-perfect) matching on the graph such that every vertex in  $T$  is part of the match.

Revisiting Equation 1, let  $D_c$  be a  $cM^2 \times M^2$  matrix in which the the rows are duplicated  $c$  times. The  $M^2 \times cM^2$  assignment from the permuted image to the source is, as before, a  $(0,1)$ -matrix  $P_c$  with exactly one 1 in each row and at most one 1 in each column. We still have:

16 × 16 tiles				
original	prompt	copies = 1,5,10		
	a tea cup			
	a young boy			
	a tea cup			
	a young boy			
32 × 32 tiles				
	Great Wave			
	a magpie			
	Great Wave			
	a magpie			

**Fig. 14:** Any number of image copies can be used as the basis. In each of the examples, we look at 1,5 and 10 copies of the original to create the prompt. Top Table: 16 × 16 tiles and prompts: of “a tea cup” and “a young boy” created with the *Mona Lisa* and *Starry Night*. Bottom Table: 32 × 32 tiles and prompts of: “a magpie” and “The Great Wave off Kanagawa” created with Mondrian-like squares and *Girl with the Pearl Earring*.



$$\min_{P_c} \text{tr}(P_c D_c) \quad (4)$$

Here, we define the trace of a non-square matrix  $A$  with shape  $(a_1, a_2)$  as  $\text{tr}(A) = \sum_{i=1}^{\min(a_1, a_2)} a_{ii}$ . The solution is implemented as the non-square variant of the Kuhn-Munkres algorithm. Results are shown in Figure 14 (see column copies=5 & copies=10). Finally, as a further extension to this approach, we note that  $c$  can be set *per tile*, thereby allowing fine-grained control over the specific tiles that should appear more often in the results.

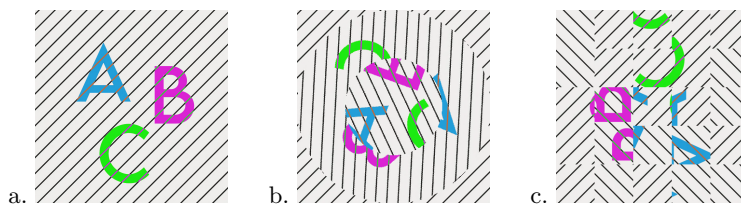
A straightforward variation of using multiple copies of the same image as the source material is using multiple *different* images as the source material. This easily fits into the framework presented in this section with minimal changes; selections of tiles from any of the basis images are allowed for each position in the synthesized image.

## 5.2 Alternate Transformations

To this point, we have focused upon the Permutation transformation. This transformation worked particularly well since using the Kuhn-Munkres algorithm provided a known, and efficient, method for matching tiles in multiple images.

Here, we demonstrate that the procedure of interleaving diffusion’s denoising step with energy minimization matching is general and works across other transformations. We will demonstrate this using Concentric Rings and Flips. For both, we are able to use simple greedy and efficient matching procedures.

In the Concentric Rings transformation, we place  $C$  concentric rings, each with equal radial size, around the center of the image. The rings can be rotated independently to transform image A into image B, see Figure 15b. Analogously to the work in the previous sections, the rotations of the rings are not pre-specified. Instead, the best rotation of the rings is computed at every mainline step using the rolled-out images. Differences between corresponding rings in image A and B are computed and their sum is minimized.



**Fig. 15:** Two transforms are shown here. The first is the *Concentric Rings transformation*. Here, concentric circles are rotated independently; the original, shown in (a), is rotated with 2 concentric circles, shown in (b). Second, the *Flips transformation*, allows for horizontal flips and 4-cardinal rotations of blocks at various resolutions in the image pyramid. In (c), the image is flipped at the largest resolution and various flips and rotations are done independently for various blocks at the  $5 \times 5$  division level.

Results are shown in Figure 16, middle three rows. Here, we evaluated 72 rotations for each ring (in  $5^\circ$  increments) independently of the other rings. The larger the number of rings that were used, the clearer the results.

For the Flip transformation, we experimented with tile rotation and mirroring effects at multiple levels in the image pyramid. Given a division,  $d$ , we divide the original square image into  $d \times d$  equal sized blocks. The allowed manipulations for each block are a flip (horizontally) and rotation by  $(0^\circ, 90^\circ, 180^\circ, 270^\circ)$ . Rather than doing this at a single level, we allow this to happen at several divisions,  $D$ . For example, a division set  $D = (1, 5)$ , where the full image can be modified as well as at the  $\frac{1}{5}$  boundaries, might yield a result as shown in Figure 15c.

Results are shown in Figure 16, bottom two rows. For simplicity, we only allowed two resolutions of operation: the entire image, and the lowest resolution (shown in each row). This first provides a mechanism to make a global change, and the second a mechanism for smaller, local, changes.

Though it is difficult to make quantitative, general, statements on these qualitative results, we provide a few observations. In general, the original Permutation transformation provided the most compelling results. The permutations of tiles has two attributes that we suspect are important. First, the permutation itself provides a substantial amount of freedom of movement. Blocks can be moved throughout the image, thereby allowing very different images to be created from the same set of pixels. Second, the movement keeps together most spatially localized pixels. As natural images exhibit a high amount of spatial cohesiveness, moving entire blocks preserves patches of consistent colors and textures.

The Concentric Rings transformation does substantially better with more rings. However, note that each ring rotation (especially in the outer rings) controls the position of spatially disparate pixels and the region of a single ring manipulation may extend the full width of the image. This necessitates creating images using potentially unnatural constraints.

The Flips transformation, on the other hand, maintains spatial cohesiveness. In the examples shown, we allowed flips & rotations at full and at either  $8 \times 8$  or  $16 \times 16$  blocks. In our initial trials, we experimented with not including the full level transformation. If the top level was omitted, the system often failed in creating two recognizable distinct images. In the extreme, although very fine-grained tiling adds parameters to the transformation, it results in excessively local changes that make it impossible to create noticeably different images – there is an empirical compromise between  $d = 1$  global changes and very fine-grained tiling. Allowing the  $d = 1$  global change also helped ameliorate locality effects. Nevertheless, the constraints on this transformation are far more restrictive than on the Permutation transformation.

## 6 Conclusions & Discussion

Simply by rearranging an image’s tiles, we presented methods to transform an image into a novel one of any subject matter. This method extends and improves recent work in generation of optical illusions in four fundamental aspects.



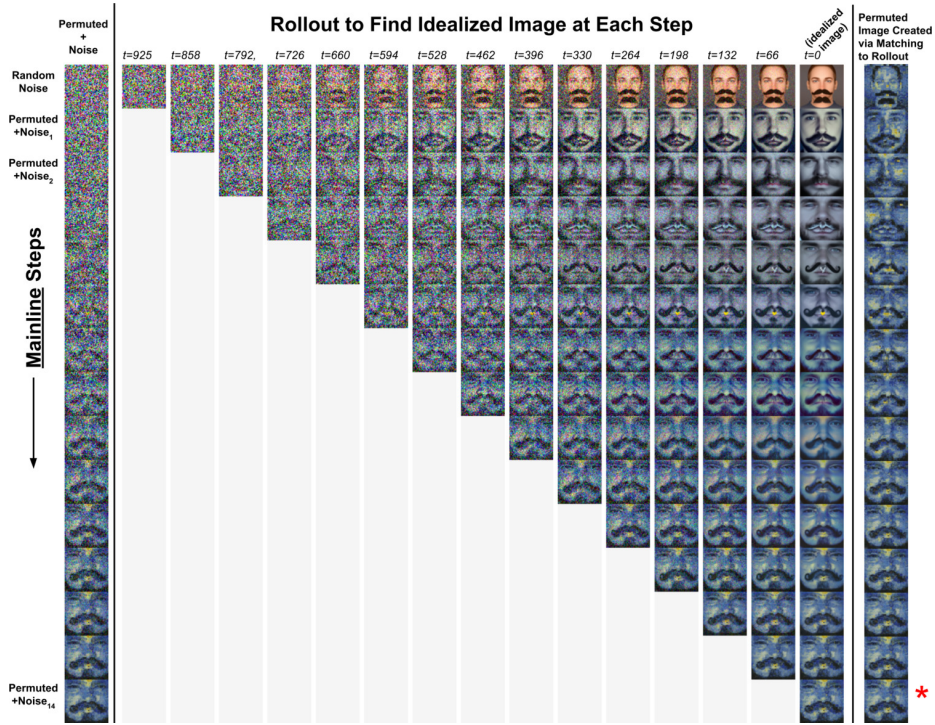
**Fig. 16:** Results for the Permutation, Concentric Rings and Flips transformations using similar prompts. Horizontal pairs are transforms of one another using the transformation in the left column.

1. **The arrangement of tiles need not be *a priori* specified.** Rather, through a dynamic matching step, the arrangement is jointly created with the image. Beyond creating qualitatively and quantitatively better images, this opens new functionality.
2. **A source image can be pre-specified.** Previously, all images had to be created by the process to allow their content to be matched. Dynamic matching removes that constraint, allowing a user-specified source image.
3. **The problem becomes *easier* as the number of tiles grows;** the opposite was true with static matching.
4. **An infinite number of copies** of the source image can be used in matching. Multiple different images can also be used for the source.

We have extended this study to parameterized transforms beyond randomized-patch permutations. The interleaving of energy minimization and de-noising applies equally well to a variety of transforms.

Looking forward, we note that though this work presented results on a vision-processing / graphics task, in a broader sense, the system was a method to navigate a system of constraints. Understanding the use of the diffusion process to search through the valid spaces in this potentially alternate category of problems remains an exciting prospect for future work.

## 7 Appendix



**Fig. 17:** Rollout visualization. The mainline progress is shown on the left, progressing vertically downwards. For each mainline step, a rollout that begins with the current mainline image computes the idealized image for the prompt, “A Man with a Mustache”. Once the idealized image is found, dynamic matching finds the best permutation  $\psi_t$  that matches the  $16 \times 16$  blocks from the idealized image to the  $\beta$  image, *Starry Night* by Van Gogh. Noise is added as shown in Figure 8. The process is then repeated. The final image is shown with a red asterisk.

## References

1. Amir, D., Weiss, Y.: Understanding and simplifying perceptual distances. In: Proceedings of the IEEE/CVF Conference on Computer Vision and Pattern Recognition. pp. 12226–12235 (2021) [5](#)
2. Avrahami, O., Lischinski, D., Fried, O.: Blended diffusion for text-driven editing of natural images. In: Proceedings of the IEEE/CVF Conference on Computer Vision and Pattern Recognition. pp. 18208–18218 (2022) [2](#)
3. Bar-Tal, O., Yariv, L., Lipman, Y., Dekel, T.: Multidiffusion: Fusing diffusion paths for controlled image generation (2023) [3](#)
4. Burgert, R., Li, X., Leite, A., Ranasinghe, K., Ryoo, M.S.: Diffusion illusions: Hiding images in plain sight (2023) [2](#)
5. Chen, Z., Geng, D., Owens, A.: Images that sound: Composing images and sounds on a single canvas (2024) [2](#)
6. Croitoru, F.A., Hondru, V., Ionescu, R.T., Shah, M.: Diffusion models in vision: A survey. *IEEE Transactions on Pattern Analysis and Machine Intelligence* (2023) [2](#)
7. Das, K.K.: Role of pre-embedded associated memory in generation of optical illusions. *J Psychol Cognition* **3**(2) (2018) [1](#)
8. Dhariwal, P., Nichol, A.: Diffusion models beat gans on image synthesis. *Advances in neural information processing systems* **34**, 8780–8794 (2021) [2](#)
9. Elsayed, G., Shankar, S., Cheung, B., Papernot, N., Kurakin, A., Goodfellow, I., Sohl-Dickstein, J.: Adversarial examples that fool both computer vision and time-limited humans. In: Bengio, S., Wallach, H., Larochelle, H., Grauman, K., Cesa-Bianchi, N., Garnett, R. (eds.) *Advances in Neural Information Processing Systems*. vol. 31. Curran Associates, Inc. (2018), [https://proceedings.neurips.cc/paper\\_files/paper/2018/file/8562ae5e286544710b2e7ebe9858833b-Paper.pdf](https://proceedings.neurips.cc/paper_files/paper/2018/file/8562ae5e286544710b2e7ebe9858833b-Paper.pdf) [1](#)
10. Everaert, M.N., Bocchio, M., Arpa, S., Süssstrunk, S., Achanta, R.: Diffusion in style. In: Proceedings of the IEEE/CVF International Conference on Computer Vision (ICCV). pp. 2251–2261 (October 2023) [2](#)
11. Freeman, W.T., Adelson, E.H., Heeger, D.J.: Motion without movement. *ACM Siggraph Computer Graphics* **25**(4), 27–30 (1991) [2](#)
12. Geng, D., Park, I., Owens, A.: Visual anagrams: Generating multi-view optical illusions with diffusion models. arXiv:2311.17919 (November 2023), <https://arxiv.org/abs/2311.17919> [2](#), [4](#), [5](#), [6](#), [11](#), [14](#)
13. Geng, D., Park, I., Owens, A.: Factorized diffusion: Perceptual illusions by noise decomposition (2024) [2](#), [3](#)
14. Goodfellow, I.J., Shlens, J., Szegedy, C.: Explaining and harnessing adversarial examples. arXiv preprint arXiv:1412.6572 (2014) [1](#)
15. Hendrycks, D., Zhao, K., Basart, S., Steinhardt, J., Song, D.: Natural adversarial examples. In: Proceedings of the IEEE/CVF Conference on Computer Vision and Pattern Recognition (CVPR). pp. 15262–15271 (June 2021) [1](#)
16. Ho, J., Jain, A., Abbeel, P.: Denoising diffusion probabilistic models. In: *Advances in Neural Information Processing Systems 33: Annual Conference on Neural Information Processing Systems 2020, NeurIPS 2020, December 6-12, 2020, virtual* (2020), <https://proceedings.neurips.cc/paper/2020/hash/4c5bcfec8584af0d967f1ab10179ca4b-Abstract.html> [4](#), [9](#)
17. Ho, J., Salimans, T.: Classifier-free diffusion guidance. arXiv:2207.12598 (2022) [4](#)
18. Hsiao, K.W., Huang, J.B., Chu, H.K.: Multi-view wire art. *ACM Trans. Graph.* **37**(6), 242 (2018) [2](#)

19. Jaini, P., Clark, K., Geirhos, R.: Intriguing properties of generative classifiers (2024) [1](#)
20. Kuhn, H.W.: The hungarian method for the assignment problem. *Naval research logistics quarterly* **2**(1-2), 83–97 (1955) [4](#), [6](#)
21. Liu, N., Li, S., Du, Y., Torralba, A., Tenenbaum, J.B.: Compositional visual generation with composable diffusion models (2023) [2](#)
22. Lo, C., Dinov, I.: Investigation of optical illusions on the aspects of gender and age. *UCLA USJ* **24** (2011) [1](#)
23. Midjourney: Midjourney. <https://midjourney.com> (2024), accessed: 2024-5-22 [2](#)
24. Mitra, N.J., Pauly, M.: Shadow art. *ACM Transactions on Graphics* **28**(5), 156–1 (2009) [2](#)
25. Munkres, J.: Algorithms for the assignment and transportation problems. *Journal of the society for industrial and applied mathematics* **5**(1), 32–38 (1957) [4](#), [6](#)
26. Ngo, J., Sankaranarayanan, S., Isola, P.: Is CLIP fooled by optical illusions? (2023), <https://openreview.net/forum?id=YdGkE4Ugg2C> [1](#)
27. Nichol, A., Dhariwal, P., Ramesh, A., Shyam, P., Mishkin, P., McGrew, B., Sutskever, I., Chen, M.: Glide: Towards photorealistic image generation and editing with text-guided diffusion models. *arXiv preprint arXiv:2112.10741* (2021) [2](#)
28. Oliva, A., Torralba, A., Schyns, P.G.: Hybrid images. *ACM Transactions on Graphics (TOG)* **25**(3), 527–532 (2006) [1](#), [2](#)
29. Radford, A., Kim, J.W., Hallacy, C., Ramesh, A., Goh, G., Agarwal, S., Sastry, G., Askell, A., Mishkin, P., Clark, J., et al.: Learning transferable visual models from natural language supervision. In: *International Conference on Machine Learning*. pp. 8748–8763. PMLR (2021) [6](#), [8](#)
30. Ramesh, A., Pavlov, M., Goh, G., Gray, S., Voss, C., Radford, A., Chen, M., Sutskever, I.: Zero-shot text-to-image generation. In: *International Conference on Machine Learning*. pp. 8821–8831. PMLR (2021) [2](#)
31. Rombach, R., Blattmann, A., Lorenz, D., Esser, P., Ommer, B.: High-resolution image synthesis with latent diffusion models. In: *Proceedings of the IEEE/CVF conference on computer vision and pattern recognition*. pp. 10684–10695 (2022) [11](#)
32. Rombach, R., Blattmann, A., Lorenz, D., Esser, P., Ommer, B.: High-resolution image synthesis with latent diffusion models (2021) [2](#), [9](#)
33. Saharia, C., Chan, W., Saxena, S., Li, L., Whang, J., Denton, E., Ghasemipour, S.K.S., Ayan, B.K., Mahdavi, S.S., Lopes, R.G., Salimans, T., Ho, J., Fleet, D.J., Norouzi, M.: Photorealistic text-to-image diffusion models with deep language understanding (2022). <https://doi.org/10.48550/ARXIV.2205.11487>, <https://arxiv.org/abs/2205.11487> [2](#)
34. Saharia, C., Chan, W., Saxena, S., Li, L., Whang, J., Denton, E.L., Ghasemipour, K., Gontijo Lopes, R., Karagol Ayan, B., Salimans, T., et al.: Photorealistic text-to-image diffusion models with deep language understanding. *Advances in neural information processing systems* **35**, 36479–36494 (2022) [2](#)
35. Shonenkov, A., Konstantinov, M., Bakshandaeva, D., Schuhmann, C., Ivanova, K., Klokova, N.: If by deepfloyd lab at stabilityai. <https://github.com/deep-floyd/IF> (2023), accessed: 2024-5-22 [2](#), [4](#)
36. Song, J., Meng, C., Ermon, S.: Denoising diffusion implicit models. *arXiv preprint arXiv:2010.02502* (2020) [2](#)
37. Tancik, M.: Illusion-diffusion. <https://github.com/tancik/Illusion-Diffusion> (2023), accessed: 2024-5-22 [2](#)
38. Tumanyan, N., Geyer, M., Bagon, S., Dekel, T.: Plug-and-play diffusion features for text-driven image-to-image translation. In: *Proceedings of the IEEE/CVF Conference on Computer Vision and Pattern Recognition*. pp. 1921–1930 (2023) [2](#)

39. de Wit, M.M., van der Kamp, J., Withagen, R.: Visual illusions and direct perception: Elaborating on gibson's insights. *New Ideas in Psychology* **36**, 1–9 (2015)  
[1](#)